^{18}F-Fluoromisonidazole Kinetic Modeling for Characterization of Tumor Perfusion and Hypoxia in Response to Antiangiogenic Therapy

Milan Grkovski[1], Sally-Ann Emmas[2], and Sean D. Carlin[3]

[1]Department of Medical Physics, Memorial Sloan Kettering Cancer Center, New York, New York; [2]Imaging Team, Personalised Healthcare and Biomarkers, AstraZeneca, Macclesfield, United Kingdom; and [3]Department of Radiology, Memorial Sloan Kettering Cancer Center, New York, New York

Multiparametric imaging of tumor perfusion and hypoxia with dynamic ^{18}F-fluoromisonidazole (^{18}F-FMISO) PET may allow for an improved response assessment to antiogenic therapies. Cediranib (AZD2171) is a potent inhibitor of tyrosine kinase activity associated with vascular endothelial growth factor receptors 1, 2, and 3, currently in phase II/III clinical trials. Serial dynamic ^{18}F-FMISO PET was performed to investigate changes in tumor biomarkers of perfusion and hypoxia after cediranib treatment. **Methods:** Twenty-one rats bearing HT29 colorectal xenograft tumors were randomized into a vehicle-treated control group (0.5% methylcellulose daily for 2 d [5 rats] or 7 d [4 rats]) and a cediranib-treated test group (3 mg/kg daily for 2 or 7 d; 6 rats in both groups). All rats were imaged before and after treatment, using a 90-min dynamic PET acquisition after administration of 42.1 ± 3.9 MBq of ^{18}F-FMISO by tail vein injection. Tumor volumes were delineated manually, and the input function was image-derived (abdominal aorta). Kinetic modeling was performed using an irreversible 1-plasma 2-tissue compartmental model to estimate the kinetic rate constants K_1, K_1/k_2, and k_3—surrogates for perfusion, ^{18}F-FMISO distribution volume, and hypoxia-mediated entrapment, respectively. Tumor-to-blood ratios (TBRs) were calculated on the last dynamic frame (80–90 min). Tumors were assessed ex vivo by digital autoradiography and immunofluorescence for microscopic visualization of perfusion (pimonidazole) and hypoxia (Hoechst 33342). **Results:** Cediranib treatment resulted in significant reduction of mean voxelwise ^{18}F-FMISO TBR, K_1, and K_1/k_2 in both the 2-d and the 7-d groups ($P < 0.05$). The k_3 parameter was increased in both groups but reached significance only in the 2-d group. In the vehicle-treated groups, no significant change in TBR, K_1, K_1/k_2, or k_3 was observed ($P > 0.2$). Ex vivo tumor analysis confirmed the presence of hypoxic tumor regions that nevertheless exhibited relatively lower ^{18}F-FMISO uptake. **Conclusion:** ^{18}F-FMISO kinetic modeling reveals a more detailed response to antiogenic treatment than a single static image is able to reveal. The reduced mean K_1 reflects a reduction in tumor vascular perfusion, whereas the increased k_3 reflects a rise in hypoxia-mediated entrapment of the radiotracer. However, if only late static images are analyzed, the observed reduction in ^{18}F-FMISO uptake after treatment with cediranib may be mistakenly interpreted as a global decrease, rather than an increase, in tumor hypoxia. These findings support the use of ^{18}F-FMISO kinetic modeling to more accurately characterize the response to treatments that have a direct effect on tumor vascularization and perfusion.

Key Words: ^{18}F-FMISO; hypoxia; perfusion; kinetic modeling; cediranib; antiangiogenesis

Targeting of tumor neovasculature has a potential to limit cancer progression and has led to the development of antiogenic drugs approved for treatment of various human malignancies (*1*). Treatments that normalize or even promote blood vessel growth may enhance drug delivery to tumors (*2*) and sensitize them to chemotherapy (*3*). Such agents may also exacerbate hypoxia, which in turn facilitates treatment resistance by promoting neovascularization and regrowth of a more belligerent tumor phenotype (*1,2*) and is associated with poor overall survival (*4*). Recent studies that were aimed at alleviating tumor hypoxia while improving tumor perfusion suggested an enhanced outcome in radio-, chemo- and immunotherapies (*1*).

Cediranib (AZD2171) is a novel, orally administered multi–vascular endothelial growth factor receptor inhibitor (*5*) that is currently being tested as a maintenance treatment for patients with platinum-sensitive relapsed ovarian cancer. Cediranib affects tumor growth by acutely impeding blood flow to the tumor and results in a dose-dependent growth inhibition (*5*). However, to reach the full potential of antiogenic therapies, clinically relevant patient stratification is crucial. Successful implementation of window-of-opportunity trials (*6*) that may help select effective drug combinations for specific patients at earlier stages during treatment requires accurate monitoring of treatment response and nuanced understanding of the tumor biology.

^{18}F-fluoromisonidazole (^{18}F-FMISO) is the most widely used PET radiotracer for noninvasive, quantitative, reproducible, and clinically feasible imaging of tumor hypoxia (*7–11*). However, ^{18}F-FMISO PET scans are usually performed in static mode (*9*), which does not allow for the simultaneous assessment of blood flow and ^{18}F-FMISO distribution volume and may result in either underestimation or overestimation of the degree of tumor hypoxia (*12*). Multiparametric imaging presents an attractive opportunity for evaluating treatment response (*13*). Several studies have reported the added benefit of assessing both tumor perfusion and

hypoxia in predicting response to therapy, suggesting that such metrics may have independent value for tumor characterization and treatment adaptation (14,15).

Simultaneous assessment of tumor perfusion and hypoxia can be achieved through kinetic modeling of dynamic ^{18}F-FMISO PET scans and carries several benefits. First, uncoupling the contribution of hypoxia-mediated entrapment to the total ^{18}F-FMISO signal results in a more accurate estimation of tumor hypoxia, since the variations in the ^{18}F-FMISO distribution volume combined with structurally and functionally abnormal vasculature may lead to low uptake in hypoxic regions or high uptake in normoxic regions even at later times after injection (12,16). Second, assessment of tumor perfusion is clinically relevant, as it is an indirect measure of angiogenesis and the delivery of nutrients and systemic agents to the tumor and may help in elucidating response mechanisms to both systemic and targeted treatments (17). Since ^{18}F-FMISO passively diffuses out of the vasculature and through cell membranes because of its lipophilicity, early ^{18}F-FMISO uptake correlates with tumor perfusion as measured with the reference standard, ^{15}O-H$_2$O PET (18). We hypothesized that kinetic modeling of dynamic ^{18}F-FMISO PET clarifies the ambiguity in interpreting static ^{18}F-FMISO uptake after angiogenic therapy by decoupling the contributions of hypoxia-mediated entrapment and ^{18}F-FMISO distribution volume to total signal.

MATERIALS AND METHODS

### Animal Preparation, Imaging, and Treatment

All animal experiments and procedures were approved by our Institutional Animal Care and Use Committee and complied with the National Institutes of Health regulations on the research use of rodents.

Tumor inoculation (19), ^{18}F-FMISO production (20), and the dynamic PET imaging protocol (21) have been described previously. In brief, approximately 5.0×10^6 HT29 human colorectal carcinoma cells (catalog no. HTB-38; American Type Culture Collection) were subcutaneously injected into the right hind limb of 6- to 8-wk-old female athymic *nu/nu* rats. Twenty-one animals bearing tumors between 200 and 1,500 mm^3 were used in the study. The animals were anesthetized with 2% isoflurane in air, and a 90-min baseline dynamic PET acquisition (4×5-, 4×10-, 4×30-, 7×60-, 10×300-, and 3×600-s frames) was initiated simultaneously with the administration of 42.1 ± 3.9 MBq of ^{18}F-FMISO via tail vein injection. Imaging studies were performed with either a microPET R4 or a microPET Focus-120 small-animal scanner (Siemens Medical Solutions Inc.).

Subsequently, the animals were randomly distributed into a vehicle-treated control group (0.5% methylcellulose daily for 2 d [5 rats] or 7 d [4 rats]) and a cediranib-treated group (3 mg/kg daily for 2 or 7 d; $n = 6$ in both groups) (Fig. 1). Cediranib and vehicle were administered by oral gavage (19). The bioactivity of the selected cediranib dosage was confirmed in our previous studies using the same tumor model (19). After the treatment period, 90-min follow-up dynamic PET scans were performed for all groups. All animals were administered pimonidazole hydrochloride (60 mg/kg; Natural Pharmacia International, Inc.) and Hoechst 33342 (2 mg in 100 μL of phosphate-buffered saline; Sigma Aldrich) via the tail vein at 90 and 5 min before sacrifice, respectively.

Histology and Autoradiography

After posttreatment imaging, the animals were sacrificed and an angiocatheter placed in the tumor perpendicular to the coronal plane to preserve tumor orientation during sectioning. The tumors were excised and embedded in optimal-cutting-temperature mounting
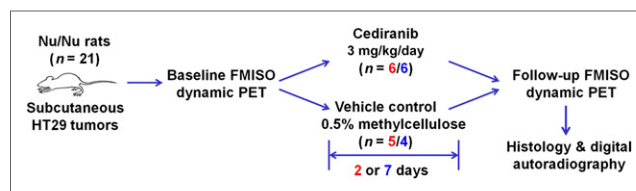
FIGURE 1. Experimental schematic. Animals bearing colorectal carcinoma xenografts were imaged with dynamic ^{18}F-FMISO PET at baseline and subsequently randomized into cediranib and vehicle groups. After completion of treatment, second dynamic ^{18}F-FMISO PET scan was obtained, followed by ex vivo analysis of tumor specimens.

medium (Sakura Finetek) frozen on dry ice, and series of 10-μm frozen sections were immediately cut. To determine radiotracer distribution, digital autoradiography was performed by placing tissue sections in a film cassette against a phosphor imaging plate (Fujifilm BAS-MS2325; Fuji Photo Film) for 6 h at −20°C. Phosphor imaging plates were read at a pixel resolution of 50 μm with a BAS-1800II bioimaging analyzer (Fujifilm Medical Systems). After autoradiographic exposure, the same frozen sections were then used for fluorescence staining and microscopy.

Immunofluorescence staining for pimonidazole was performed as previously described (22) using a rabbit polyclonal antipimonidazole primary antibody (1:40 dilution, catalog no. 2627; Natural Pharmacia International, Inc.). Secondary detection was performed using goat antirabbit Alexa-488 (20 μg/mL; Invitrogen) in blocking buffer. Images were acquired at ×40 magnification using a BX60 fluorescence microscope (Olympus America, Inc.) equipped with a motorized stage (Prior Scientific Instruments Ltd.) and a CC12 camera (Olympus). Whole-tumor montage images were obtained by acquiring multiple fields at ×40 magnification, followed by alignment using MicroSuite Biological Suite (version 2.7; Olympus). Sequential tumor sections were stained with hematoxylin and eosin, and bright-field images were acquired in the same manner as above.

Kinetic Modeling

Voxelwise kinetic modeling of dynamic ^{18}F-FMISO PET images was performed in PMOD (version 3.604; PMOD Technologies GmbH) using an irreversible 1-plasma 2-tissue compartmental model (21). The analysis was focused on the kinetic rate constants k_3, a surrogate for hypoxia-mediated entrapment (12,16); K_1, a surrogate for perfusion (18); and K_1/k_2, a surrogate for ^{18}F-FMISO distribution volume. k_4 was set to 0, reflecting irreversible trapping of ^{18}F-FMISO (7). Assuming unit density tissue, k_3 and K_1 are expressed in min^{-1}, whereas K_1/k_2 is unitless. The image-derived input function was obtained by segmenting the descending aorta in the initial 3 frames of the study (0–15 s). Image-derived input function time–activity curves were corrected for partial-volume effects and fitted with a 3-term exponential function, as described previously (21). Tumors were delineated manually on a slice-by-slice basis on the final frame (80–90 min), with tumor dimensions as measured with a caliper serving as a guideline. Tumor-to-blood ratio (TBR) was derived from the last time frame, using the measured activity concentration in the image-derived input function volume of interest as the reference for blood activity concentration. Since ^{18}F-FMISO exhibits irreversible trapping, the standard Patlak formulation (23) can be used to express the TBR as

$$\text{TBR} = \frac{K_1 k_3}{k_2 + k_3} \cdot \frac{\int_0^t C_p(\tau)d\tau}{C_p(t)} + \text{DV}, \qquad \text{Eq. 1}$$

where $C_p(t)$ describes the ^{18}F-FMISO activity concentration in plasma, and DV is the ^{18}F-FMISO distribution volume, approximated

by K_1/k_2. ^{18}F-FMISO equilibration time, T^*, after which unbound ^{18}F-FMISO has reached more than 99% of its final ratio relative to blood, was calculated as

$$T^\star = 7 \cdot \frac{\ln(2)}{(k_2 + k_3)}. \qquad \text{Eq. 2}$$

Calculation of kinetic rate constants on a voxel level was performed using the 2-tissue compartmental model with ridge-regression fitting as implemented in the PXMOD tool of PMOD.

Statistical Analysis

Comparisons of investigated metrics between the vehicle- and cediranib-treated groups was performed with the unpaired 2-tailed Student t test, assuming a significance level of $P < 0.05$. The Pearson correlation coefficient, r, was used to calculate the correlation between the parameters of interest.

RESULTS

Mean animal weight and tumor volume ($\pm$SD) at baseline was 216 $\pm$ 20 g and 529 $\pm$ 345 mm^3, respectively ($n = 21$). Tumor volume did not significantly change in any of the 4 groups (Table 1). Analysis of static PET images (a single frame acquired between 80 and 90 min after ^{18}F-FMISO injection) revealed a significant reduction in SUV$_{mean}$ and SUV$_{max}$ in both the 2-d and the 7-d cediranib groups relative to baseline measurements (Table 1). No significant difference was observed in either of the vehicle groups.

Kinetic modeling of dynamic PET data revealed a more detailed picture of ^{18}F-FMISO behavior. In the cediranib groups, significant reductions were observed in both K_1 (from 0.13 to 0.07 min^{-1} for 2-d and from 0.24 to 0.08 min^{-1} for 7-d) and K_1/k_2 (from 1.12 to 0.71 for 2-d and from 1.21 to 0.91 for 7-d), whereas in the vehicle groups no significant differences in these parameters could be observed (Table 2). For k_3, a significant increase was observed in the 2-d cediranib group (from 0.0009 to 0.0069 min^{-1}). An increase in the k_3 parameter in the 7-d cediranib group (from 0.0039 to 0.0050 min^{-1}) was not significant, partially due to the wide spread of mean tumor k_3 values on the baseline scan. The

latter is exemplified on the box-and-whisker plots, shown in Figure 2 for all groups and for all investigated kinetic rate constants. Changes in TBR mirrored the SUV data, with significant reductions observed in the cediranib groups (17% and 24% for 2- and 7-d, respectively) but not in the vehicle groups. ^{18}F-FMISO equilibration time was found to be less than 90 min in all groups, confirming the sufficiency of the acquisition duration.

Representative parametric maps of TBR, k_3, K_1, and K_1/k_2 at baseline and follow-up for a cediranib-treated animal are shown in Figure 3. Although mean intratumor TBR dropped from 1.44 at baseline to 1.29 after treatment, mean intratumor k_3 (calculated by averaging the voxelwise k_3 values) increased from 0.0022 to 0.0069 min^{-1}, indicating an actual increase in hypoxia-mediated entrapment of ^{18}F-FMISO. The decrease in TBR can be explained by both decreased perfusion due to pruning of intratumor vessels (mean intratumor K_1 dropped from 0.15 to 0.08 min^{-1}) and decreased ^{18}F-FMISO distribution volume (mean intratumor K_1/k_2 dropped from 1.16 to 0.86).

The discordance between k_3 and TBR as surrogate markers for tumor hypoxia is further highlighted in k_3–TBR scatterplots for two animals, one from a cediranib group (7-d; Fig. 4A) and the other from a vehicle group (2-d; Fig. 4B). Although, in the vehicle animal, Pearson r between voxelwise values of k_3 and TBR was high and remained relatively unchanged (decreasing from 0.85 to 0.73), the corresponding r in the cediranib animal decreased substantially from 0.65 at baseline to -0.45 after treatment. The decrease in TBR in the latter case was not due to a decrease in k_3 or a long ^{18}F-FMISO equilibration time but to a decrease in ^{18}F-FMISO distribution volume. Results confirming the foregoing observations were observed when the k_3–TBR correlation was calculated on a whole-tumor level (i.e., by taking mean voxelwise k_3 and TBR for each animal). Pearson r changed from 0.63 to 0.51 in vehicle animals (to achieve higher statistics, the two vehicle groups were pooled into a single group), whereas for cediranib animals (pooled data including both the 2-d and the 7-d groups), it changed substantially, from 0.66 to -0.39.

Ex vivo analysis of tumor sections provided further detail on the distribution of ^{18}F-FMISO in the cediranib and vehicle groups.

TABLE 1
Tumor Volume, SUV$_{mean}$, and SUV$_{max}$ Before and After Treatment with Cediranib or Vehicle for 2 or 7 Days

Length of treatment	Volume (mm³)		SUV$_{mean}$		SUV$_{max}$	
	Before	After	Before	After	Before	After
2 d						
Cediranib ($n = 6$)	330 ± 63	345 ± 53	0.52 ± 0.04	0.39 ± 0.08	0.96 ± 0.09	0.73 ± 0.18
P	0.67		0.01*		0.03*	
Vehicle ($n = 5$)	526 ± 378	518 ± 422	0.53 ± 0.05	0.49 ± 0.07	1.05 ± 0.15	1.00 ± 0.20
P	0.98		0.11		0.36	
7 d						
Cediranib ($n = 6$)	700 ± 297	604 ± 248	0.56 ± 0.17	0.38 ± 0.08	0.99 ± 0.32	0.71 ± 0.19
P	0.56		0.01		0.01*	
Vehicle ($n = 4$)	577 ± 556	931 ± 982	0.58 ± 0.18	0.52 ± 0.21	1.07 ± 0.31	0.92 ± 0.46
P	0.55		0.40		0.30	

*Statistically significant.

TABLE 2
^{18}F-FMISO Kinetic Modeling Before and After Treatment with Cediranib or Vehicle for 2 or 7 Days

| Length of treatment	K_1 (min^{-1}) Before	After	k_3 (min^{-1}) Before	After	K_1/k_2 Before	After	TBR$_{mean}$ Before	After	T^* (min) Before	After
2 d										
Cediranib (n = 6)	0.13 ± 0.05	0.07 ± 0.03	0.0009 ± 0.0011	0.0069 ± 0.0023	1.12 ± 0.17	0.71 ± 0.13	1.28 ± 0.09	1.06 ± 0.20	44 ± 12	58 ± 25
P	0.02*		<0.01*		<0.01*		0.03*		0.24	
Vehicle (n = 5)	0.14 ± 0.08	0.17 ± 0.09	0.0040 ± 0.0027	0.0032 ± 0.0022	0.90 ± 0.13	0.91 ± 0.18	1.24 ± 0.20	1.22 ± 0.12	40 ± 21	29 ± 14
P	0.46		0.62		0.51		0.87		0.39	
7 d										
Cediranib (n = 6)	0.24 ± 0.07	0.08 ± 0.02	0.0039 ± 0.0039	0.0050 ± 0.0032	1.21 ± 0.16	0.91 ± 0.23	1.66 ± 0.16	1.27 ± 0.15	25 ± 6	55 ± 7
P	<0.01*		0.60		0.02*		<0.01*		<0.01*	
Vehicle (n = 4)	0.19 ± 0.05	0.16 ± 0.04	0.0027 ± 0.0026	0.0046 ± 0.0032	1.18 ± 0.15	1.14 ± 0.19	1.42 ± 0.07	1.53 ± 0.10	32 ± 6	34 ± 4
P	0.40		0.39		0.78		0.11		0.65	

*Statistically significant.

Representative examples of coregistered images showing ^{18}F-FMISO digital autoradiographs, immunofluorescence staining, and hematoxylin and eosin staining are shown for HT29 xenograft tumors excised from cediranib and vehicle animals (Fig. 5 and Supplemental Fig. 1; supplemental materials are available at http://jnm.snmjournals.org). The tumors were generally characterized by largely necrotic centers containing islands of viable cells (seen with hematoxylin and eosin staining), well-perfused rims (evidenced by Hoechst 33342 staining [blue]), and an extensive perinecrotic hypoxic region staining positively for the exogenous hypoxia tracer pimonidazole (green). In the tumors of the vehicle group, ^{18}F-FMISO distribution closely corresponded to the spatial pattern of pimonidazole uptake. Islands of viable tumor extending to the boundary of the necrotic region were clearly visualized by pimonidazole immunofluorescence staining and by ^{18}F-FMISO digital autoradiographs. Analysis of tumors from the cediranib groups revealed some notable differences from the vehicle-group tumors. There was a loss of correspondence between pimonidazole staining in some, generally centrally located, tumor regions, with these regions being characterized by strong pimonidazole staining but weak, or absence of, staining for Hoechst 33342.

Also of note was an absence of ^{18}F-FMISO uptake in these regions. In contrast, the peripheral regions of these tumors generally showed a strong correspondence between ^{18}F-FMISO uptake and pimonidazole staining. The noncorrespondence of pimonidazole and ^{18}F-FMISO in the cediranib groups is explained by the large difference in the concentrations administered (approximately 220 μM and 4.8 pM for pimonidazole and ^{18}F-FMISO, respectively), greatly reducing the sensitivity of pimonidazole to changes in tracer delivery relative to ^{18}F-FMISO.

DISCUSSION

This study was performed to explore the use of ^{18}F-FMISO as an imaging biomarker for the acute effects of antiangiogenic therapies and to investigate which imaging metrics most accurately reflect the underlying changes in tumor physiology caused by these treatments. Sustained angiogenesis is one of the hallmarks of
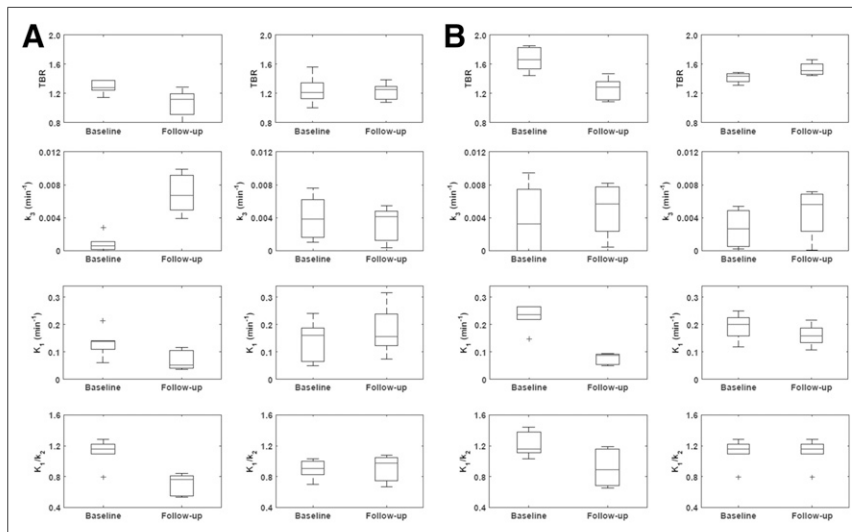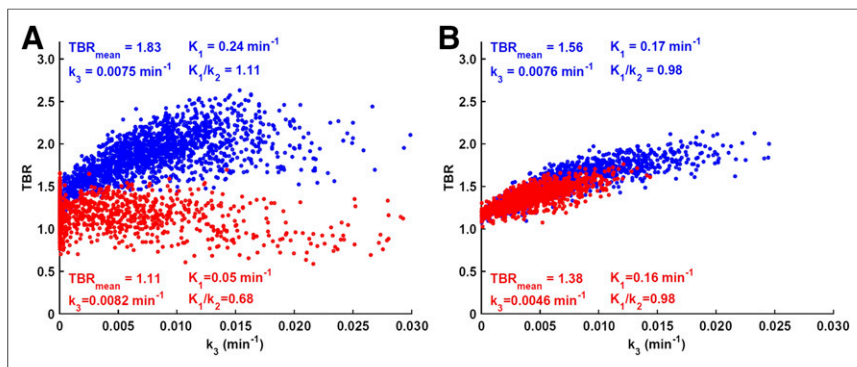

FIGURE 2. (A) Box-and-whisker plots summarizing mean intratumor values of TBR, k_3, K_1, and K_1/k_2 for animals treated 2 d with cediranib (left panels) or 2 d with vehicle (right panels). (B) Corresponding plots for animals treated for 7 d with cediranib (left panels) or 7 d with vehicle (right panels).
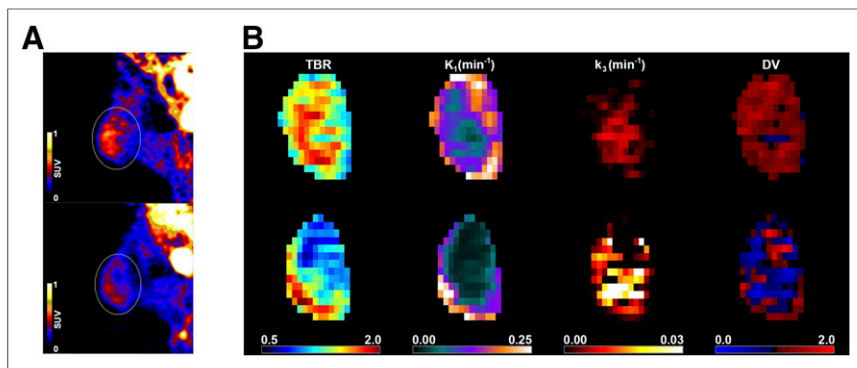
FIGURE 3. (A) Single-slice, midtumor PET images obtained 90 min after injection from representative animal in 7-d cediranib group at baseline (left) and after treatment (right). (B) Intratumor voxelwise maps (coronal view) derived from dynamic PET images of same animal at baseline (top row) and after treatment (bottom row). DV = distribution volume.

cancer, and the targeting and exploitation of tumor neovasculature provide an additional pharmaceutical option for disease management. However, many antiangiogenic drugs have a complex effect on tumor blood supply and oxygen delivery, with an acute reduction in tumor perfusion being followed by a longer process of vascular normalization (*24*). This initial effect may facilitate an acute hypoxic response, in turn fueling tumor progression (*1*), and may have important implications for the optimal scheduling of concurrent radiation therapy. Accurate characterization of tumor perfusion and hypoxia may therefore prove to be an important consideration for patient stratification before therapy and for modification of therapy after its onset.

^{18}F-FMISO PET is the most extensively evaluated technique for noninvasive, quantitative imaging of tumor hypoxia (*9*). Bartlett et al., working with a prostate-tumor model, concluded that kinetic modeling of dynamic ^{18}F-FMISO PET data provides additional information otherwise unavailable from static images and that the k_3 parameter is better at identifying low tissue oxygen than are other measures of ^{18}F-FMISO uptake (*16*). Recently, we demonstrated that kinetic modeling of dynamic ^{18}F-FMISO PET data can clarify the ambiguity in interpreting static ^{18}F-FMISO uptake in patients with head and neck cancer (*12*).

The presented findings support the conclusion of the foregoing study, indicating that kinetic modeling of dynamic ^{18}F-FMISO PET data allows for a more detailed assessment of response to an antiangiogenic agent than can be achieved through a single static image. The observation of decreased total ^{18}F-FMISO SUV relative to baseline (Table 1) implies a cediranib-mediated reduction in tumor hypoxia. However, kinetic analysis revealed that in at least a fraction of tumor voxels, the rate of hypoxia-specific entrapment of ^{18}F-FMISO (k_3) actually increases (Table 2; Fig. 2). We observed a large drug-dependent reduction in vascular delivery of ^{18}F-FMISO (K_1) that reflects similar reductions we and others have observed in delivery of gadolinium contrast agent as measured using dynamic MRI (*25,26*). We also observed reductions in ^{18}F-FMISO distribution volume as shown by K_1/k_2, which may reflect the higher fraction of necrotic cells after treatment. Parametric mapping revealed heterogeneous responses to cediranib, with peripheral voxels showing a reduction in K_1 and K_1/k_2, whereas voxels with a higher k_3 tended to be seen in more centrally located tumor regions (Fig. 3).

Although, for the vehicle group, k_3 and TBR were relatively well correlated, both on a voxel-by-voxel level and on a whole-tumor level, treatment with cediranib decreased the k_3–TBR correlation substantially (Fig. 4). These results indicate that when antiangiogenic drugs are administered, static ^{18}F-FMISO uptake metrics may not accurately reflect the underlying hypoxia status. TBR depends not only on k_3 but also on K_1/k_2 (^{18}F-FMISO distribution volume) and T^* (^{18}F-FMISO equilibration time). By pruning the tumor vessels and increasing the fraction of nonviable tumor cells (causing reduced K_1/k_2), ^{18}F-FMISO may appear to decrease after antiangiogenic therapy despite constant or even increasing levels of tumor hypoxia, leading to an incorrect assessment of tumor response. Under normoxic conditions ($k_3 = 0$), TBR will reflect the ^{18}F-FMISO distribution volume (Eq. 1). Consequently, K_1/k_2 has a potential to bias the assessment of ^{18}F-FMISO uptake if only static scans are used (*12*). For treated animals, K_1/k_2 was consistently lower than 1, resulting in lower TBRs that underestimate the degree of intratumor hypoxia. ^{18}F-FMISO equilibration time was found to be less than 90 min in all groups; therefore, lower total ^{18}F-FMISO uptake was not caused by tumor hypoperfusion.

The foregoing observations are supported by ex vivo digital autoradiography and immunofluorescence staining of tumor sections. In vehicle-treated animals, an inverse relationship with the vascular perfusion marker Hoechst 33342 was found for areas staining positively for pimonidazole. ^{18}F-FMISO autoradiography exhibited a strong positive correspondence with pimonidazole uptake, as expected. In the cediranib-treated animals, many of the centrally located regions of viable tissue did not show a significant accumulation of ^{18}F-FMISO,
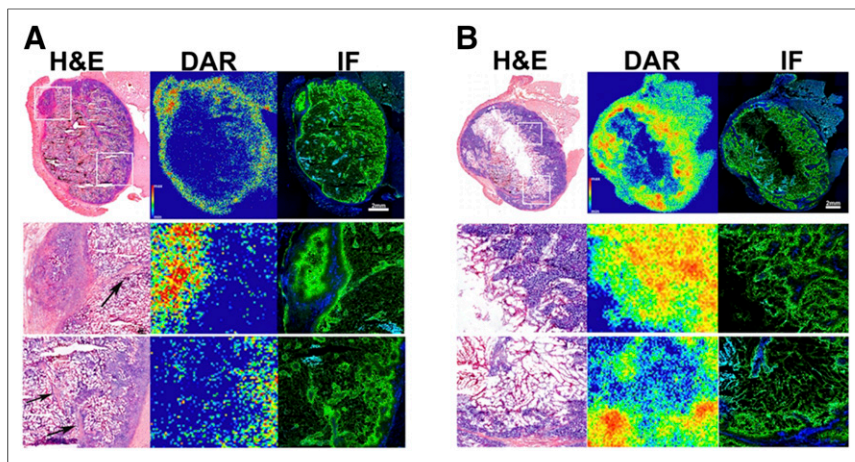

FIGURE 4. (A) Correlation between k_3 and TBR, two surrogate markers of tumor hypoxia, for representative animal in 7-d cediranib group. Pearson r between k_3 and TBR changed substantially, from 0.65 on baseline scan (blue) to −0.45 at follow-up (red), whereas T^* increased from 22 to 60 min, respectively. (B) Corresponding scatterplot for representative animal in 2-d vehicle group. Pearson r between k_3 and TBR changed only slightly, from 0.85 on baseline scan (blue) to 0.73 at follow-up (red), whereas T^* remained relatively unchanged (27 and 29 min, respectively).

FIGURE 5. Hematoxylin and eosin (H&E), digital autoradiography (DAR), and immunofluorescence (IF) (green = pimonidazole, blue = Hoechst 33342) analysis of ex vivo tumor sections. Upper and lower zoom regions are indicated on whole-mount hematoxylin and eosin images. (A) Tumors in the cediranib group showed viable central regions positive for pimonidazole but lacking ^{18}F-FMISO uptake (black arrows). (B) Tumors in the vehicle group showed strong correspondence between pimonidazole staining and ^{18}F-FMISO uptake in both central and peripheral regions.

despite showing uptake of pimonidazole. ^{18}F-FMISO signal was observed mainly in the tumor periphery, localized adjacent to regions of high Hoechst 33342 staining, without the clear correspondence with pimonidazole seen in tumors of the vehicle groups. These distributions imply that uptake of ^{18}F-FMISO in the central tumor region is reduced—even though these regions remain hypoxic—and reflects the reduced K_1 and elevated k_3 parameters observed from kinetic modeling.

Although pimonidazole and ^{18}F-FMISO were coadministered approximately 90 min before sacrifice, these similarly structured hypoxia tracers provided divergent information in the cediranib-treated groups. This divergence can be explained by the high molar concentration of pimonidazole administered (approximately 220 μM) and by the binary nature of the immunofluorescence-based detection of pimonidazole adducts. These factors render identification of hypoxic tumor regions based on pimonidazole much less sensitive to fluctuations in vascular tracer delivery than that based on ^{18}F-FMISO, for which a much lower concentration is given (~4.8 pM) and for which absolute uptake is measured. Although differences in the respective Po_2 sensitivity of the hypoxia tracers, and the potential that a partial-volume effect will reduce apparent ^{18}F-FMISO activity, are also possible explanations for this observation, neither of these effects was observed in the tumors of the vehicle groups, suggesting that the influence of these phenomena is likely small.

The results of this study go some way to explaining the divergent and occasionally confounding data on the effect that antiangiogenic agents have on tumor hypoxia and ^{18}F-FMISO imaging response. There are multiple reports of observations that antiangiogenic agents can increase tumor hypoxia by promoting vessel pruning and inhibiting neoangiogenesis (27–29), often determined using immunohistochemistry markers of tumor hypoxia. In contrast, there are also several reports of a reduction in ^{18}F-FMISO uptake after antiangiogenic treatment (30–34). Differences in antiangiogenic compounds, tumor types, and experimental methodologies make it difficult to draw a definitive conclusion. However, our data suggest that although metrics derived from static scans are attractive because of the simple acquisition protocols, ^{18}F-FMISO uptake may not directly reflect changes in intratumor hypoxia unless radiotracer delivery and distribution are also accounted for. For this reason, we believe that the use of dynamic acquisition protocols should be considered when tumor perfusion and tracer distribution are directly affected by the treatment under evaluation. Clarifying the relative contributions of tracer distribution, tumor perfusion, and tumor hypoxia to total ^{18}F-FMISO signal yields multiparametric imaging data that can better elucidate the acute response and mechanisms of resistance to antiangiogenic therapy and may better inform optimal drug dosing and treatment scheduling.

CONCLUSION

^{18}F-FMISO kinetic modeling reveals a more detailed response to cediranib treatment than a single static image is able to reveal. Reduced mean K_1 reflects a reduction in vascular perfusion, whereas increased k_3 reflects a rise in hypoxia-mediated tracer entrapment. However, if only late static images from the same dataset are analyzed, the reduction in ^{18}F-FMISO uptake after cediranib treatment may be mistakenly interpreted as a global decrease, rather than an increase, in tumor hypoxia. These findings support the use of ^{18}F-FMISO kinetic modeling to more accurately characterize the response to treatments that have a direct effect on tumor vascularization and perfusion.

DISCLOSURE

REFERENCES

1. Jain RK. Antiangiogenesis strategies revisited: from starving tumors to alleviating hypoxia. *Cancer Cell.* 2014;26:605–622.
2. Rivera LB, Bergers G. Tumor angiogenesis, from foe to friend. *Science.* 2015;349:694–695.
3. Wong PP, Demircioglu F, Ghazaly E, et al. Dual-action combination therapy enhances angiogenesis while reducing tumor growth and spread. *Cancer Cell.* 2015;27:123–137.
4. Horsman MR, Mortensen LS, Petersen JB, Busk M, Overgaard J. Imaging hypoxia to improve radiotherapy outcome. *Nat Rev Clin Oncol.* 2012;9:674–687.
5. Wedge SR, Kendrew J, Hennequin LF, et al. AZD2171: a highly potent, orally bioavailable, vascular endothelial growth factor receptor-2 tyrosine kinase inhibitor for the treatment of cancer. *Cancer Res.* 2005;65:4389–4400.
6. Dubois LJ, Niemans R, van Kujik SJ, et al. New ways to image and target tumour hypoxia and its molecular responses. *Radiother Oncol.* 2015;116:352–357.
7. Koh WJ, Rasey JS, Evans ML, et al. Imaging of hypoxia in human tumors with [F-18]fluoromisonidazole. *Int J Radiat Oncol Biol Phys.* 1992;22:199–212.

8. Rasey JS, Koh WJ, Evans ML, et al. Quantifying regional hypoxia in human tumors with positron emission tomography of [18F]fluoromisonidazole: a pretherapy study of 37 patients. *Int J Radiat Oncol Biol Phys.* 1996;36:417–428.

9. Fleming IN, Manavaki R, Blower PJ, et al. Imaging tumour hypoxia with positron emission tomography. *Br J Cancer.* 2015;112:238–250.

10. Okamoto S, Shiga T, Yasuda K, et al. High reproducibility of tumor hypoxia evaluated by 18F-fluoromisonidazole PET for head and neck cancer. *J Nucl Med.* 2013;54:201–207.

11. Grkovski M, Schwartz J, Rimner A, et al. Reproducibility of 18F-fluoromisonidazole intratumour distribution in non-small cell lung cancer. *EJNMMI Res.* 2016;6:79.

12. Grkovski M, Lee NY, Schöder H, et al. Multiparametric imaging of tumor hypoxia and perfusion with 18F-FMISO dynamic PET in head and neck cancer. *J Nucl Med.* February 9, 2017 [Epub ahead of print].

13. Padhani AR, Miles KA. Multiparametric imaging of tumor response to therapy. *Radiology.* 2010;256:348–364.

14. Lehtiö K, Eskola O, Viljanen T, et al. Imaging perfusion and hypoxia with PET to predict radiotherapy response in head-and-neck cancer. *Int J Radiat Oncol Biol Phys.* 2004;59:971–982.

15. Thorwarth D, Eschmann SM, Scheiderbauer J, Paulsen F, Alber M. Kinetic analysis of dynamic 18F-fluoromisonidazole PET correlates with radiation treatment outcome in head-and-neck cancer. *BMC Cancer.* 2005;5:152.

16. Bartlett RM, Beattie BJ, Naryanan M, et al. Image-guided Po2 probe measurements correlated with parametric images derived from 18F-fluoromisonidazole small-animal PET data in rats. *J Nucl Med.* 2012;53:1608–1615.

17. Rajendran JG, Mankoff DA. Positron emission tomography imaging of blood flow and hypoxia in tumors. In: Shields AF, Price P, eds. *In Vivo Imaging of Cancer Therapy.* Totowa, NJ: Humana Press; 2007.

18. Bruehlmeier M, Roelcke U, Schubiger PA, Ametamey SM. Assessment of hypoxia and perfusion in human brain tumors using PET with 18F-fluoromisonidazole and 15O-H2O. *J Nucl Med.* 2004;45:1851–1859.

19. Bokacheva L, Kotedia K, Reese M, et al. Response of HT29 colorectal xenograft model to cediranib assessed with 18F-fluoromisonidazole positron emission tomography, dynamic contrast-enhanced and diffusion-weighted MRI. *NMR Biomed.* 2013;26:151–163.

20. Lim JL, Berridge MS. An efficient radiosynthesis of [18F]fluoromisonidazole. *Appl Radiat Isot.* 1993;44:1085–1091.

21. Grkovski M, Schwartz J, Gönen M, et al. Feasibility of 18F-fluoromisonidazole kinetic modeling in head and neck cancer using shortened acquisition times. *J Nucl Med.* 2016;57:334–341.

22. Carlin S, Zhang H, Reese M, et al. A comparison of the imaging characteristics and microregional distribution of 4 hypoxia PET tracers. *J Nucl Med.* 2014; 55:515–521.

23. Patlak CS, Blasberg RG. Graphical evaluation of blood-to-brain transfer constants from multiple-time uptake data: generalizations. *J Cereb Blood Flow Metab.* 1985;5:584–590.

24. Jain RK, Duda DG, Willett CG, et al. Biomarkers of response and resistance to antiangiogenic therapy. *Nat Rev Clin Oncol.* 2009;6:327–338.

25. Bradley DP, Tessier JL, Checkley D, et al. Effects of AZD2171 and vandetanib (ZD6474, Zactima) on haemodynamic variables in an SW620 human colon tumour model: an investigation using dynamic contrast-enhanced MRI and the rapid clearance blood pool contrast agent, P792 (gadomelitol). *NMR Biomed.* 2008;21:42–52.

26. Bradley DP, Tessier JJ, Lacey T, et al. Examining the acute effects of cediranib (RECENTIN, AZD2171) treatment in tumor models: a dynamic contrast-enhanced MRI study using gadopentate. *Magn Reson Imaging.* 2009;27:377–384.

27. Rapisarda A, Melillo G. Overcoming disappointing results with antiangiogenic therapy by targeting hypoxia. *Nat Rev Clin Oncol.* 2012;9:378–390.

28. Ulivi P, Marisi G, Passardi A. Relationship between hypoxia and response to antiangiogenic therapy in metastatic colorectal cancer. *Oncotarget.* 2016;7:46678–46691.

29. Pham E, Yin M, Peters CG, et al. Preclinical efficacy of bevacizumab with CRLX101, an investigational nanoparticle–drug conjugate, in treatment of metastatic triple-negative breast cancer. *Cancer Res.* 2016;76:4493–4503.

30. Thézé B, Bernards N, Beynel A, et al. Monitoring therapeutic efficacy of sunitinib using [18F]FDG and [18F]FMISO PET in an immunocompetent model of luminal B (HER2-positive)-type mammary carcinoma. *BMC Cancer.* 2015;15:534.

31. Hernández-Agudo E, Mondejar T, Soto-Montenegro ML, et al. Monitoring vascular normalization induced by antiangiogenic treatment with 18F-fluoromisonidazole PET. *Mol Oncol.* 2016;10:704–718.

32. Diaz R, Nguewa PA, Redardo M, Manrique I, Calvo A. Sunitinib reduces tumor hypoxia and angiogenesis, and radiosensitizes prostate cancer stem-like cells. *Prostate.* 2015;75:1137–1149.

33. Valable S, Petit E, Roussel S, et al. Complementary information from magnetic resonance imaging and 18F-FMISO positron emission tomography in the assessment of the response to an antiangiogenic treatment in a rat brain tumor model. *Nucl Med Biol.* 2011;38:781–793.

34. Hugonnet F, Fournier L, Medioni J, et al. Metastatic renal cell carcinoma: relationship between initial metastasis hypoxia, change after 1 month's sunitinib, and therapeutic response: an 18F-fluoromisonidazole PET/CT study. *J Nucl Med.* 2011;52:1048–1055.